2016-12-28

Evaluating models of Coulomb stress transfer: Is variable fault geometry important?

Mildon, Zoe

10.1002/2016GL071128
Geophysical Research Letters
American Geophysical Union

AGU PUBLICATIONS

Geophysical Research Letters

RESEARCH LETTER
10.1002/2016GL071128

Key Points:
- Current Coulomb stress models of planar faults are not representative of true fault geometries
- New method presented here creates strike-variable faults from many rectangular patches that works within *Coulomb 3.4*
- There are substantial differences between planar versus strike-variable fault transferred stresses so past earthquakes should be re-examined

Supporting Information:
- Supporting Information S1

Correspondence to:
Z. K. Mildon,
zoe.mildon.13@ucl.ac.uk

Citation:
Mildon, Z. K., S. Toda, J. P. Faure Walker, and G. P. Roberts (2016), Evaluating models of Coulomb stress transfer: Is variable fault geometry important?, *Geophys. Res. Lett.*, *43*, doi:10.1002/2016GL071128.

Received 7 SEP 2016
Accepted 8 DEC 2016
Accepted article online 12 DEC 2016

Evaluating models of Coulomb stress transfer: Is variable fault geometry important?

Zoe K. Mildon[1], Shinji Toda[2], Joanna P. Faure Walker[1], and Gerald P. Roberts[3]

[1]Institute for Risk and Disaster Reduction, University College London, London, UK, [2]International Research Institute of Disaster Science, Tohoku University, Sendai, Japan, [3]Department of Earth and Planetary Sciences, Birkbeck, University of London, London, UK

Abstract To determine the importance of receiver fault geometry in Coulomb stress calculations a new methodology is presented to model faults with variable geometry. Although most models use planar faults, it is known that these are inaccurate representations of faults observed in the field. The central Italian Apennines are chosen as a straightforward tectonic system with well-exposed normal faults to investigate the effect of variable geometry. It is shown that the static Coulomb stress transfer is most sensitive to changes in strike of the receiver faults, rather than changes in dip and rake. Therefore, a novel methodology to generate strike-variable faults composed of discrete rectangular patches is developed. Using the 2009 L'Aquila earthquake ($M_w = 6.3$) the calculated stress transferred to planar versus variable faults is assessed. The stress transferred to variable faults is sufficiently different when compared to planar cases to merit other earthquake sequences being reassessed with available fault geometry.

1. Introduction

Coulomb stress transfer [*Harris and Simpson*, 1992; *Reasenberg and Simpson*, 1992; *King et al.*, 1994] is routinely calculated following large earthquakes (recent examples include Gorkha, $M_w = 7.8$, 2015 [*Diao et al.*, 2015]; L'Aquila, $M_w = 6.3$ [*Walters et al.*, 2009], and Emilia-Romagna, $M_w = 6.1$, 2012 [*Saraò and Peruzza*, 2012]). In each of these examples, the Coulomb stress is calculated from a planar source fault and resolved onto planar receiver faults. However, the fault maps in these areas [*Decelles et al.*, 2001; *U.S. Geological Survey, and California Geological Survey*, 2006; *Basili et al.*, 2008] show that these surface fault traces are not straight; therefore, a planar model is an inaccurate representation of the fault geometry at depth. Efforts to include variable fault geometry have been made prior to this study, including using triangular dislocation elements [*Parsons et al.*, 1999; *Meade*, 2007; *Bie and Ryder*, 2014]. In this paper we investigate the effect of including variable source and receiver fault geometry (as rectangular elements) on the Coulomb stress calculation by using *Coulomb 3.4* [*Lin and Stein*, 2004; *Toda et al.*, 2005].

Coulomb stress transfer may be calculated either by resolving onto receiver faults of a known location and orientation [e.g., *Toda et al.*, 1998], onto generalized faults of a specified orientation [e.g., *Lin and Stein*, 2004, Figure 13] or onto optimally orientated planes [e.g., *King et al.*, 1994]. In this paper, we only consider the first approach in order to compare the difference between planar and strike-variable faults. It has long been established that when performing stress calculations the mean strike and dip of the receiver faults are important. However, what has not been routinely included is the use of variable strikes and dips along a single fault within Coulomb modeling. This is demonstrated in *Lin and Stein* [2004] for a strike-slip earthquake and two types of receiver faults, strike-slip and thrust faults, in different orientations. This example uses planar faults, despite the published fault traces being variable: the Coalinga anticline [*Namson and Davis*, 1988], White Wolf reverse fault [*Stein and Thatcher*, 1981], Garlock strike-slip fault [*Dokka and Travis*, 1990], and the San Andreas fault [*U.S. Geological Survey, and California Geological Survey*, 2006]. Despite this, there are few examples of Coulomb stress transfer models using nonplanar fault geometries (some examples are *Jiang et al.* [2013] and *Bie and Ryder* [2014]). These examples use a triangular mesh approach outlined in *Meade* [2007]. This approach has not been widely adopted, and a simple rectangular fault, even discretized into numerous small patches, is still the standard approach to calculate the Coulomb stress transfer. This paper presents a methodology to model variable fault strike that has been developed for rapid use within *Coulomb* and has been tested rigorously to ensure that the results calculated are robust.

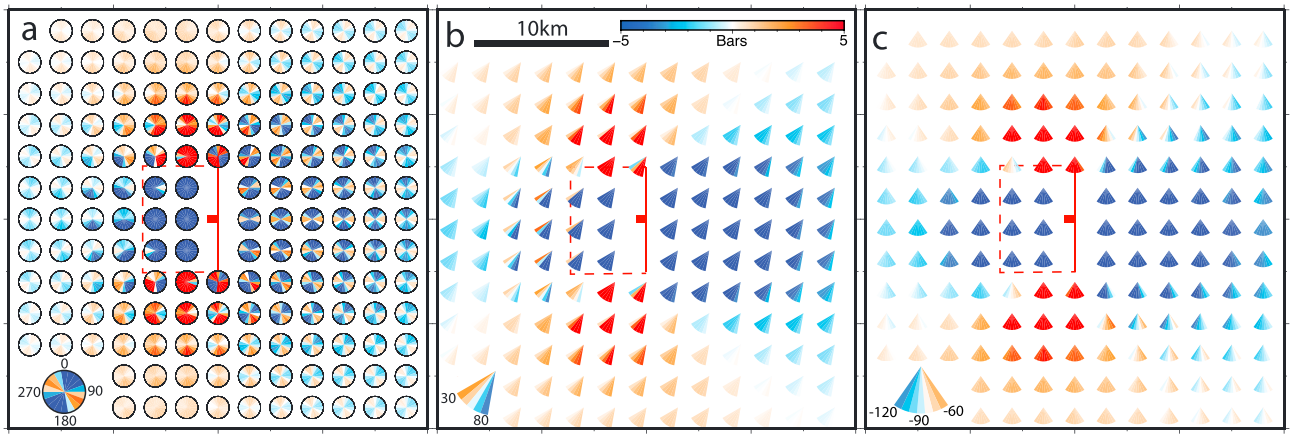

Figure 1. Testing the sensitivity of the Coulomb stress transfer to variations in the three geometry parameters. The solid red line is the surface trace of the source fault, and the dashed red line is the extent of the source fault to depth. The distance and stress scales are constant across all tests. The orientation of the coloured wedges for each plot corresponds to the stress transferred to a fault with the same strike, dip, or rake. (a) Strike sensitivity test. In the immediate hanging wall directly above the extent of the source fault, the stress transferred is totally insensitive to the strike (solid blue circles), but in the footwall the stress changes from positive to negative with small changes in strike indicating high sensitivity. The dip and rake remain constant (65° and −90°, respectively). (b) Dip sensitivity test. Slight sensitivity is seen in the hanging wall, but otherwise, most regions around the source fault are relatively insensitive (solid blue/red wedges). The strike and rake remain constant (180° and −90°, respectively). (c) Rake sensitivity test. Most regions around the source fault are insensitive (solid blue/red wedges); areas of moderate sensitivity are at 45° into the footwall from the tips of the source fault. The strike and dip remain constant (180° and 65°, respectively). Hence, the Coulomb stress is most sensitive to changes in strike of the receiver faults.

In order to assess the importance of fault geometry, the Italian Apennines is used as case study region. This area of continental crust is undergoing extension at ~3mm/yr [*Hunstad et al.*, 2003; *Serpelloni et al.*, 2005; *D'Agostino et al.*, 2009; *Faure Walker et al.*, 2010] which is distributed across a soft-linked array of normal faults [*Cowie and Roberts*, 2001]. No other faulting styles are widely recognized in the field with Holocene activity. Hence, the central Apennines is a relatively uncomplicated tectonic setting with one dominant style of faulting, and we are able to assess the effect of variable geometry on Coulomb stress transfer without having to consider different faulting styles. Throughout the central Apennines, normal faults are exposed at the surface as limestone bedrock scarps. These have formed over numerous earthquake cycles since the end of the Last Glacial Maximum (LGM, 15 ± 3ka) due to a decrease in erosion rates relative to throw rates since the LGM [*Roberts and Michetti*, 2004; *Tucker et al.*, 2011]. These scarps can be mapped, and the changes in the geometry (strike, dip, and rake) and throw can be measured from meter to kilometer resolution [*Boncio et al.*, 1996; *Piccardi et al.*, 1999; *Bonini et al.*, 2003; *Roberts and Michetti*, 2004; *Papanikolaou et al.*, 2005; *Roberts*, 2007; *Faure Walker et al.*, 2009; *Wilkinson et al.*, 2015; *Mildon et al.*, 2016]. Hence, the geometry of the normal faults can be well constrained by using the gathered field data, and the effects of including variable fault geometry into Coulomb stress calculations can be assessed. The 2009 L'Aquila ($M_w = 6.3$) earthquake is used as an example to calculate the static Coulomb stress transfer onto the surrounding faults and to compare the planar and variable fault geometry approach.

2. Coulomb Stress Sensitivity to Receiver Fault Geometry

There are three parameters that are used to describe the geometry of a fault: strike, dip, and rake (slip direction). Sensitivity tests have been performed for each parameter independently to identify the spatial sensitivity of Coulomb stress transfer around a source fault.

A simple pure dip-slip normal source fault is used for the test (180°/65°/−90° for the strike/dip/rake following the convention of *Aki and Richards* [1980], 10 km long with 2 m of uniform slip), and the Coulomb stress is calculated at a depth of 5 km. The coefficient of apparent friction used μ' [*King et al.*, 1994] is 0.4. For the receiver faults, each geometry parameter is varied individually through a range of values (strike: 0 to 360°, dip: 30 to 80°, rake: −60 to −120°), while the other two parameters are kept constant and equal to the source fault. The limits of each parameter are based on the range of values seen in the Apennines for normal faults. The results of each test are shown in Figure 1. Other depths and values of μ' have been tested and are shown in

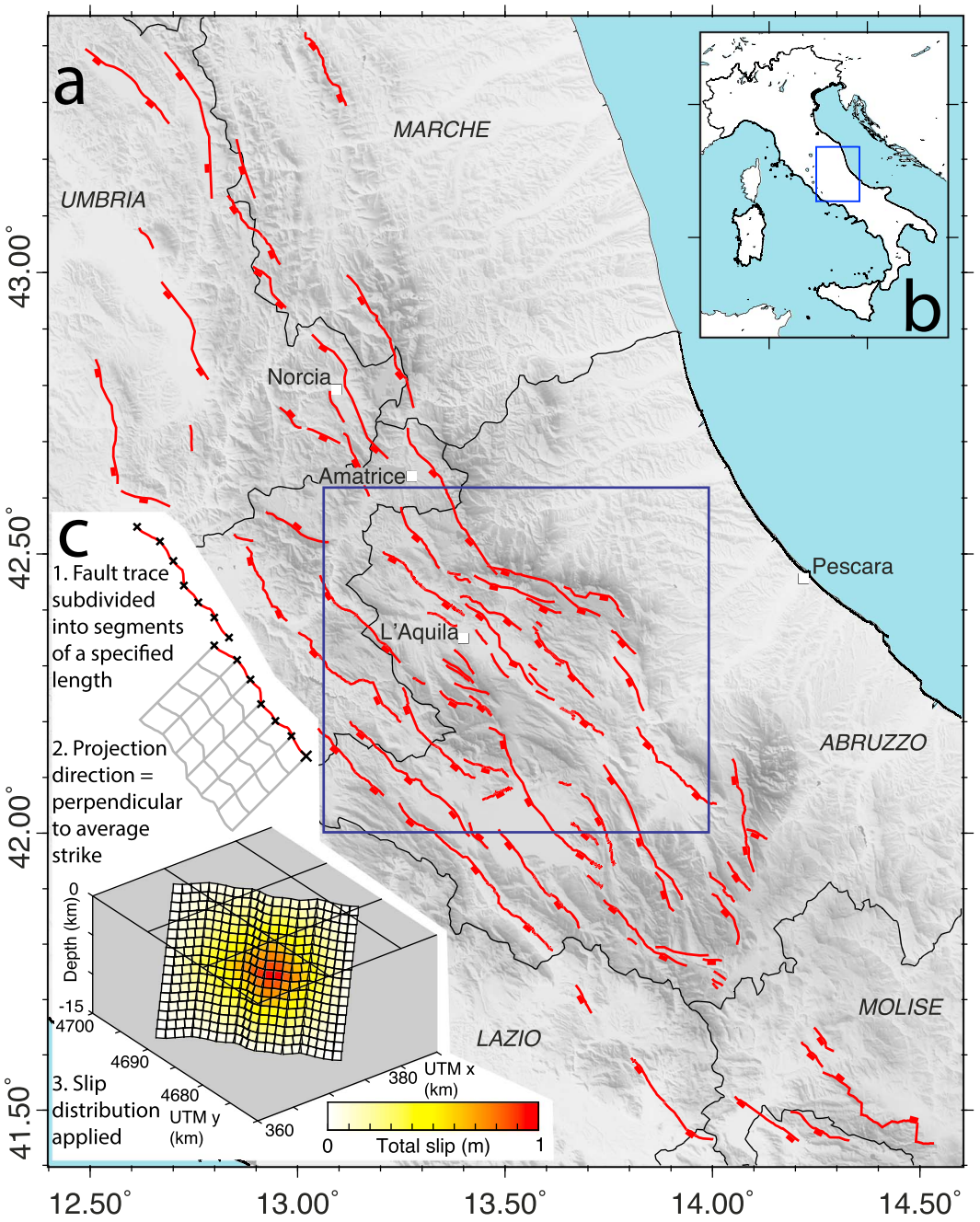

Figure 2. Summary map of the Italian Apennines and the method of generating the 3-D strike-variable faults. (a) Map of the central Apennines. The red lines are active fault traces; the red boxes indicate direction of dip. Relief is shown from low to high in grey scale and illuminated from the south-west. The thin black lines mark regional borders, and regions are named in italics. The dark blue box shows the extent of Figure 3. (b) Inset figure of Italy. The blue box shows the extent of Figure 2a. (c) Method of generating the 3-D strike-variable faults for use in *Coulomb 3.4*. 1. Fault trace is subdivided into segments of a specified length. For the examples shown in this paper, the specified length is 1 km. The Paganica fault that ruptured in 2009 is shown as the example. 2. Using an assigned projection direction that is perpendicular to the mean strike of the fault, the segment boundaries (shown as crosses) are projected to depth. 3. For faults that generate an earthquake, a slip distribution of a bulls-eye pattern is assigned to each element; this example is for the Paganica fault. The slip distribution shown here is used to generate Figure 3.

Figures S2–S4 in the supporting information. Areas of high sensitivity are identified where there are rapid stress changes from positive to negative as the parameter varies.

3. Methodology

Surface fault traces of normal faults in the central Apennines are drawn in Google Earth™ based on fieldwork (>10,000 measurements at >800 sites [from *Morewood and Roberts*, 2000; *Roberts and Michetti*, 2004; *Papanikolaou et al.*, 2005; *Papanikolaou and Roberts*, 2007; *Roberts*, 2008; *Faure Walker et al.*, 2010, 2012; *Wilkinson et al.*, 2015; *Mildon et al.*, 2016], satellite imagery, and geological maps). The field measurements are used to check that the strike of the surface traces drawn in Google Earth™ is a good representation of the true fault strike (for faults where there is limited field data coverage); there is good agreement between the traces and the field data.

From the fault traces drawn in Google Earth™, a projection direction is assigned to each fault; this is the direction perpendicular to the mean fault strike (because the mean rake is −90° for a normal fault) and controls the dip direction of the fault. For each fault, a single value of dip is used which is either the mean dip measured from field measurements (where available) or taken from the literature. If no information is available, a dip of 65° is assigned as the mean dip from all data [*Roberts and Michetti*, 2004]. A single value of rake is used (−90°), despite variations present in the field data. The variability in dip and rake is not modeled in full in order to isolate the effects of including the strike variability and because the sensitivity tests (Figure 1) showed that the transferred Coulomb stress has low sensitivity to the changes in the dip and rake of the receiver faults. In addition, changes in strike can be resolved readily from geological maps; hence, the importance of variations in this parameter for other fault systems can be understood and easily applied. The fault traces are divided into segments of a specified length of 1 km, and the points that divide the segments are projected to depth to create rectangular elements to be used as the input for *Coulomb*. The specified length of 1 km is chosen based on a trade-off between the level of detail and computational time. If the grid size were changed, this would only change the resolution of the stress field calculated. The faults are projected to a depth of 15 km by using a constant value of dip, the assumed depth of the brittle-ductile transition based on heat-flow modeling [*Cowie et al.*, 2013], and the termination of earthquakes [e.g., *Valoroso et al.*, 2013]. This process is done for all faults in the central Apennines in the Marche, Umbria, Abruzzo, Lazio, and Molise regions, by gridding the surface traces to a size of 1 km. Faults that are shorter than the depth of the seismogenic zone are assumed to maintain an aspect ratio of 1. This produces a model of the region shown in Figure 2 which contains >17,000 individual elements. Regional stress [*King et al.*, 1994] is not assigned for these models because it is unnecessary when the stress is being resolved onto known receiver faults. Changing the size of the elements will affect the area of the stress discrepancies that can be resolved, and decreasing the element size will rapidly increase the computation time. This code is written to generate input files for immediate use within *Coulomb* and is available on request.

The L'Aquila 2009 earthquake is used as a case study to test the importance of planar versus strike-variable receiver fault geometry. There are numerous slip distributions published for this earthquake, see *Wilkinson et al.* [2015] for a summary. The most prominent feature in all these slip distributions is that the highest slip occurs close to but southeast of the center of the fault plane and the slip forms a bulls-eye pattern around this point of maximum slip. All of these slip distributions are calculated for a planar source fault; this is not comparable to the strike-variable source fault used in the models presented in this paper. Hence, a simplified slip distribution of maximum slip skewed slightly to the southeast of the strike-variable fault plane, with zero slip at the ends and at 15 km depth is used here (Figures 2c and 3). The value of maximum slip was chosen to fit the moment magnitude of the event.

It is not geometrically possible to grid a smooth surface with variable strike using only rectangular elements (as allowed in *Coulomb*). Therefore, it is important to understand the effects of underlap and overlap between the elements on the generated stress field. Tests were undertaken to investigate the possible effects (Figure S1). It was found that any spurious stress signals are confined to the region directly above the source fault (when the Coulomb stress is calculated for a specified depth) and does not affect the Coulomb stress resolved directly onto receiver faults. Hence, these effects do not affect the results of this paper.

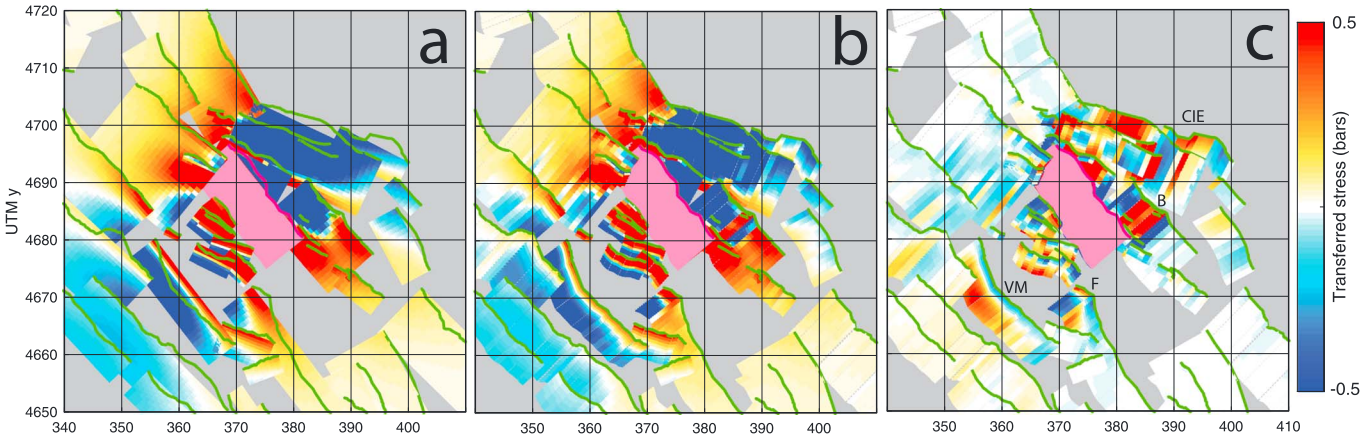

Figure 3. Comparison between Coulomb stress transferred to straight and strike-variable planar faults for the 2009 L'Aquila earthquake. The green lines show the surface expression of the receiver faults; the magenta lines show the surface expression of the Paganica (source) fault. The projection of the Paganica fault to depth is shown in pink. The outlines of each individual element are not shown for clarity; these models contain >11,000 elements. (a) Receiver and source faults modeled as segmented planar faults. The discrepancy between the mapped fault traces in green, and a planar model can be seen in this figure. (b) Receiver and source faults modeled with variable strike. The surface trace is gridded at 1 km to produce the elements. (c) The difference between the stress on variable faults and planar faults for each element in the model. Areas of faults that show large discrepancies due to the presence of bends are indicated with text and discussed in the main text. This highlights the stress patterns missed by the planar approach in Figure 3a, especially for receiver faults in the footwall (northeast) and hanging wall (southwest) of the source fault.

4. Results

4.1. Straight Versus Variable Fault Geometry

The results of Coulomb stress transfer for planar versus strike-variable faults are shown in Figure 3 for the L'Aquila 2009 earthquake. For the planar faults, the transferred stress is largely as expected for a normal fault, with receiver faults along strike from the source fault generally experiencing positive stress transfer and receiver faults across strike from the source fault experiencing negative stress. When the faults are modeled with strike-variable geometry, a similar pattern is evident, but there are notable differences between the planar and strike-variable cases. The difference in stress between the strike-variable and planar models is shown in Figure 3c. There are two main features that can be identified. The faults that show the most difference between the planar and strike-variable cases are located in the across strike from the source fault, in the footwall, and hanging wall. The areas on individual faults that show the largest differences in stress are located where there are prominent bends in the fault trace. Some examples have been highlighted in Figure 3c such as grid references 370/4670 (the tip of the Fucino fault), 395/4697 (Campo Imperatore East fault), and 385/4685 (Barisciano fault). The Velino Magnola fault has a smooth bend along its full length, and differences in stress are seen along its full length in Figure 3c. This indicates that the stress on these sections of the faults would be incorrectly resolved if modeled by the standard planar approach. Differences between the planar and strike-variable geometry cases are observed across most of Figure 3c; this shows that this is a problem across the majority of the receiver faults, especially close to the source fault and across strike.

4.2. Sensitivity Tests

The sensitivity tests shown in Figures 1 and S2–S4 show that of the parameters strike, dip, and rake, Coulomb stress transfer is most sensitive to changes in the strike of the receiver faults when the strike, dip, and rake are considered independently. Almost all regions around the source show that the stress can switch from positive to negative with changes in strike of 10–20°, except for the region directly in the hanging wall of the source fault, which is insensitive to strike. The areas that are 45° into the footwall from the tips of the fault (receiver faults in these regions would be described as being en echelon to the source fault) show especially high sensitivity where the stress switches from positive to negative around the strike of the source fault. This is important because many published models resolve the stress onto faults of exactly the same orientation as the source fault. If the actual receiver faults varied in strike by as little as 10°, then the Coulomb stress will be incorrectly calculated.

5. Discussion

The hypothesis that the Coulomb stress transferred to receiver faults is highly dependant on geometry has been reassessed and improved. Based on sensitivity tests, it is shown that different areas around the source fault are particularly sensitive to changes in different parameters of geometry. It has been shown that there are particular regions where the receiver fault geometry should either be well known or the Coulomb stress transferred should be calculated for a range of geometries. One limitation is that this method cannot be used robustly to investigate the localized stress field around the source fault because spurious stress signals may be generated. Previous examples of Coulomb stress calculations should be re-examined with this receiver fault sensitivity in mind.

Based on the high sensitivity of Coulomb stress to receiver strike, an approach to modeling normal faults with strike-variable geometry has been outlined, where the fault planes are modeled as a series of discrete rectangular patches. Using the central Italian Apennines and the L'Aquila 2009 earthquake as a case study, it has been shown that the stress resolved onto strike-variable geometry receiver faults is considerably different to the stress resolved onto discretized segmented planar faults (Figure 3c). This will have implications for the assessment of the stress transferred to the surrounding faults and the distribution of aftershocks following a major earthquake.

Although the results here are shown for a normal faulting earthquake in a relatively simple tectonic setting, similar effects are highly likely to be seen for any faulting style when the strike-variable geometry is included. Hence, any Coulomb modeling performed for any faulting style may be missing parts of the transferred stress pattern if strike-variable fault geometry is not considered where possible. Few places show such excellent fault exposure as the Italian Apennines, but this should not be considered a barrier to modeling other earthquakes and faults using this methodology. Existing fault maps from the literature, geological maps or satellite imagery can be utilized to generate variable fault planes by using the methodology outlined in this paper. The static Coulomb stress transfer of previous earthquakes and sequences should be re-examined by using this approach wherever variations in fault geometries are available.

6. Conclusions

A new methodology has been proposed to model fault planes with variable fault strike as planes composed of rectangular elements in *Coulomb 3.4*. This method has been tested rigorously and produces interesting and valid results and is available on request. This method is a powerful new approach to studying the stress transferred to receiver faults with known variable strike along their lengths. There are large discrepancies observed between a planar and a variable geometry model of faults in the Italian Apennines, with the 2009 L'Aquila earthquake shown as a case study. These discrepancies show that the transferred stress will not be uniform across a fault and regions of high stress may be generated on faults with a low average stress. These differences may better explain the locations and distributions of aftershocks and the probability and locality of the next major earthquake. Previous Coulomb stress calculations should be re-examined taking account of the receiver fault geometry wherever possible because, as demonstrated herein, the geometry has a great effect on the Coulomb stress transferred to differently orientated sections.

Acknowledgments
This study was funded by NERC Studentship award NE/L501700/1 and JSPS Short Term fellowship PE 15776. The code described in the text and in Figure 2c for generating strike-variable faults for use in *Coulomb 3.4* is available on request to the corresponding author.

References

Aki, K., and P. G. Richards (1980), *Quantitative Seismology*, 2nd ed., edited by J. Ellis, Univ. Sci. Books, New York.

Basili, R., G. Valensise, P. Vannoli, P. Burrato, U. Fracassi, S. Mariano, M. M. Tiberti, and E. Boschi (2008), The Database of Individual Seismogenic Sources (DISS), version 3: Summarizing 20 years of research on Italy's earthquake geology, *Tectonophysics*, *453*(1–4), 20–43, doi:10.1016/j.tecto.2007.04.014.

Bie, L., and I. Ryder (2014), Recent seismic and aseismic activity in the Ashikule stepover zone, NW Tibet, *Geophys. J. Int.*, *198*(3), 1632–1643, doi:10.1093/gji/ggu230.

Boncio, P., F. Brozzetti, and G. Lavecchia (1996), State of stress in the Northern Umbria-Marche Apennines (Central Italy): Inferences from microearthquake and fault kinematic analyses, *Ann. Tectonicae*, *10*, 80–97.

Bonini, M., C. Tanini, G. Moratti, L. Piccardi, and F. Sani (2003), Geological and archaeological evidence of active faulting on the Martana Fault (Umbria-Marche Apennines, Italy) and its geodynamic implications, *J. Quat. Sci.*, *18*(8), 695–708, doi:10.1002/jqs.785.

Cowie, P. A., and G. P. Roberts (2001), Constraining slip rates and spacings for active normal faults, *J. Struct. Geol.*, *23*(12), 1901–1915.

Cowie, P. A., C. H. Scholz, G. P. Roberts, J. P. Faure Walker, and P. Steer (2013), Viscous roots of active seismogenic faults revealed by geologic slip rate variations, *Nat. Geosci.*, *6*, 1036–1040, doi:10.1038/ngeo1991.

D'Agostino, N., S. Mantenuto, E. D'Anastasio, A. Avallone, M. R. Barchi, C. Collettini, F. Radicioni, A. Stoppini, and G. Fastellini (2009), Contemporary crustal extension in the Umbria–Marche Apennines from regional CGPS networks and comparison between geodetic and seismic deformation, *Tectonophysics*, *476*, 3–12, doi:10.1016/j.tecto.2008.09.033.

DeCelles, P. G., D. M. Robinson, J. Quade, T. P. Ojha, C. N. Garzione, P. Copeland, and B. N. Upreti (2001), Stratigraphy, structure, and tectonic evolution of the Himalayan fold-thrust belt in western Nepal, *Tectonics*, *20*, 487–509, doi:10.1029/2000TC001226.

Diao, F., T. R. Walter, M. Motagh, P. Prats-Iraola, R. Wang, and S. V. Samsonov (2015), The 2015 Gorkha earthquake investigated from radar satellites: Slip and stress modeling along the MHT, *Front. Earth Sci.*, *3*, 1–9, doi:10.3389/feart.2015.00065.

Dokka, R. K., and C. J. Travis (1990), Late Cenozoic strike-slip faulting in the Mojave Desert, California, *Tectonics*, *9*, 311–340, doi:10.1029/TC009i002p00311.

Faure Walker, J. P., G. P. Roberts, P. A. Cowie, I. D. Papanikolaou, P. R. Sammonds, A. M. Michetti, and R. J. Phillips (2009), Horizontal strain-rates and throw-rates across breached relay zones, central Italy: Implications for the preservation of throw deficits at points of normal fault linkage, *J. Struct. Geol.*, *31*(10), 1145–1160, doi:10.1016/j.jsg.2009.06.011.

Faure Walker, J. P., G. P. Roberts, P. R. Sammonds, and P. A. Cowie (2010), Comparison of earthquake strains over 10 2 and 10 4 year timescales: Insights into variability in the seismic cycle in the central Apennines, Italy, *J. Geophys. Res.*, *115*, B10418, doi:10.1029/2009JB006462.

Faure Walker, J. P., G. P. Roberts, P. A. Cowie, I. D. Papanikolaou, A. M. Michetti, P. R. Sammonds, M. Wilkinson, K. J. W. McCaffrey, and R. J. Phillips (2012), Relationship between topography, rates of extension and mantle dynamics in the actively-extending Italian Apennines, *Earth Planet. Sci. Lett.*, *325–326*, 76–84, doi:10.1016/j.epsl.2012.01.028.

Harris, R. A., and R. W. Simpson (1992), Changes in static stress on southern California faults after the 1992 Landers earthquake, *Nature*, *360*(6401), 251–254, doi:10.1038/360251a0.

Hunstad, I., G. Selvaggi, N. D'Agostino, P. England, P. Clarke, and M. Pierozzi (2003), Geodetic strain in peninsular Italy between 1875 and 2001, *Geophys. Res. Lett.*, *30*(4), 1181, doi:10.1029/2002GL016447.

Jiang, G., C. Xu, Y. Wen, Y. Liu, Z. Yin, and J. Wang (2013), Inversion for coseismic slip distribution of the 2010 Mw 6.9 Yushu Earthquake from InSAR data using angular dislocations, *Geophys. J. Int.*, *194*(2), 1011–1022, doi:10.1093/gji/ggt141.

King, G. C. P., R. S. Stein, and J. Lin (1994), Static stress changes and the triggering of earthquakes, *Bull. Seismol. Soc. Am.*, *84*(3), 935–953, doi:10.1016/0148-9062(95)94484-2.

Lin, J., and R. S. Stein (2004), Stress triggering in thrust and subduction earthquakes and stress interaction between the southern San Andreas and nearby thrust and strike-slip faults, *J. Geophys. Res.*, *109*, B02303, doi:10.1029/2003JB002607.

Meade, B. J. (2007), Algorithms for the calculation of exact displacements, strains, and stresses for triangular dislocation elements in a uniform elastic half space, *Comput. Geosci.*, *33*(8), 1064–1075, doi:10.1016/j.cageo.2006.12.003.

Mildon, Z. K., G. P. Roberts, J. P. Faure Walker, L. Wedmore, and K. J. W. McCaffrey (2016), Active normal faulting during the 1997 seismic sequence in Colfiorito, Umbria: Did slip propagate to the surface?, *J. Struct. Geol.*, doi:10.1016/j.jsg.2016.08.011.

Morewood, N. C., and G. P. Roberts (2000), The geometry, kinematics and rates of deformation within an en echelon normal fault segment boundary, central Italy, *J. Struct. Geol.*, *22*(8), 1027–1047, doi:10.1016/S0191-8141(00)00030-4.

Namson, J. S., and T. L. Davis (1988), Seismically active fold and thrust belt in the San Joaquin Valley, central California, *Geol. Soc. Am. Bull.*, *100*(2), 257–273, doi:10.1130/0016-7606(1988)100<0257:SAFATB>2.3.CO;2.

Papanikolaou, I. D., and G. P. Roberts (2007), Geometry, kinematics and deformation rates along the active normal fault system in the southern Apennines: Implications for fault growth, *J. Struct. Geol.*, *29*(1), 166–188, doi:10.1016/j.jsg.2006.07.009.

Papanikolaou, I. D., G. P. Roberts, and A. M. Michetti (2005), Fault scarps and deformation rates in Lazio–Abruzzo, Central Italy: Comparison between geological fault slip-rate and GPS data, *Tectonophysics*, *408*(1–4), 147–176, doi:10.1016/j.tecto.2005.05.043.

Parsons, T., R. S. Stein, R. W. Simpson, and P. A. Reasenberg (1999), Stress sensitivity of fault seismicity: A comparison between limited-offset oblique and major strike-slip faults, *J. Geophys. Res.*, *104*, 20,183–20,202, doi:10.1029/1999JB900056.

Piccardi, L., Y. Gaudemer, P. Tapponnier, and M. Boccaletti (1999), Active oblique extension in the central Apennines (Italy): Evidence from the Fucino region, *Geophys. J. Int.*, *139*(2), 499–530, doi:10.1046/j.1365-246x.1999.00955.x.

Reasenberg, P. A., and R. W. Simpson (1992), Response of regional seismicity to the static stress change produced by the loma prieta earthquake, *Science*, *255*(5052), 1687–1690, doi:10.1126/science.255.5052.1687.

Roberts, G. P. (2007), Fault orientation variations along the strike of active normal fault systems in Italy and Greece: Implications for predicting the orientations of subseismic-resolution faults in hydrocarbon reservoirs, *Am. Assoc. Petrol. Geol. Bull.*, *91*(1), 1–20, doi:10.1306/08300605146.

Roberts, G. P. (2008), Visualisation of active normal fault scarps in the Apennines, Italy: A key to assessment of tectonic strain release and earthquake rupture, *J. Virtual Explorer*, *29*(4), doi:10.3809/jvirtex.2008.00197.

Roberts, G. P., and A. M. Michetti (2004), Spatial and temporal variations in growth rates along active normal fault systems: An example from The Lazio–Abruzzo Apennines, central Italy, *J. Struct. Geol.*, *26*(2), 339–376, doi:10.1016/S0191-8141(03)00103-2.

Saraò, A., and L. Peruzza (2012), Fault-plane solutions from moment-tensor inversion and preliminary Coulomb stress analysis for the Emilia Plain, *Ann. Geophys.*, *55*(4), 647–654, doi:10.4401/ag-6134.

Serpelloni, E., M. Anzidei, P. Baldi, G. Casula, and A. Galvani (2005), Crustal velocity and strain-rate fields in Italy and surrounding regions: New results from the analysis of permanent and non-permanent GPS networks, *Geophys. J. Int.*, *161*(3), 861–880, doi:10.1111/j.1365-246X.2005.02618.x.

Stein, R. S., and W. Thatcher (1981), Seismic and aseismic deformation associated with the 1952 Kern County, California, earthquake and relationship to the Quaternary history of the White Wolf Fault, *J. Geophys. Res.*, *86*, 4913–4928, doi:10.1029/JB086iB06p04913.

Toda, S., R. S. Stein, P. A. Reasenberg, J. H. Dieterich, and A. Yoshida (1998), Stress transferred by the 1995 Mw = 6.9 Kobe, Japan, shock: Effects on aftershocks and future earthquake probabilities, *J. Geophys. Res.*, *103*, 24,543–24,565, doi:10.1029/98JB00765.

Toda, S., R. S. Stein, K. Richards-Dinger, and S. B. Bozkurt (2005), Forecasting the evolution of seismicity in southern California: Animations built on earthquake stress transfer, *J. Geophys. Res.*, *110*, B05S16, doi:10.1029/2004JB003415.

Tucker, G. E., S. W. McCoy, A. C. Whittaker, G. P. Roberts, S. T. Lancaster, and R. J. Phillips (2011), Geomorphic significance of postglacial bedrock scarps on normal-fault footwalls, *J. Geophys. Res.*, *116*, F01022, doi:10.1029/2010JF001861.

U.S. Geological Survey, and California Geological Survey (2006), Quaternary fault and fold database for the United States [online]. [Available at http//earthquakes.usgs.gov/regional/qfaults/, Accessed 28 June 2016.]

Valoroso, L., L. Chiaraluce, D. Piccinini, R. Di Stefano, D. Schaff, and F. Waldhauser (2013), Radiography of a normal fault system by 64,000 high-precision earthquake locations: The 2009 L'Aquila (central Italy) case study, *J. Geophys. Res. Solid Earth*, *118*, 1156–1176, doi:10.1002/jgrb.50130.

Walters, R. J., J. R. Elliott, N. D'Agostino, P. C. England, I. Hunstad, J. A. Jackson, B. E. Parsons, R. J. Phillips, and G. P. Roberts (2009), The 2009 L'Aquila earthquake (central Italy): A source mechanism and implications for seismic hazard, *Geophys. Res. Lett.*, *36*, L17312, doi:10.1029/2009GL039337.

Wilkinson, M., et al. (2015), Slip distributions on active normal faults measured from LiDAR and field mapping of geomorphic offsets: An example from L'Aquila, Italy, and implications for modelling seismic moment release, *Geomorphology*, *237*, 130–141, doi:10.1016/j.geomorph.2014.04.026.